



HAL
open science

Development and performance of the PIPER scalable child human body models

Philippe Beillas, Chiara Giordano, Victor Alvarez, Xiaogai Li, Xingjia Ying, Marie-Christine Chevalier, Stefan Kirscht, Svein Kleiven

► **To cite this version:**

Philippe Beillas, Chiara Giordano, Victor Alvarez, Xiaogai Li, Xingjia Ying, et al.. Development and performance of the PIPER scalable child human body models. 14th International Conference on the Protection of Children in Cars, Dec 2016, MUNICH, Germany. 19 p. hal-01720414

HAL Id: hal-01720414

<https://hal.science/hal-01720414>

Submitted on 1 Mar 2018

HAL is a multi-disciplinary open access archive for the deposit and dissemination of scientific research documents, whether they are published or not. The documents may come from teaching and research institutions in France or abroad, or from public or private research centers.

L'archive ouverte pluridisciplinaire **HAL**, est destinée au dépôt et à la diffusion de documents scientifiques de niveau recherche, publiés ou non, émanant des établissements d'enseignement et de recherche français ou étrangers, des laboratoires publics ou privés.

Development and performance of the PIPER scalable child human body models

Philippe Beillas*, Chiara Giordano**, Victor Alvarez**, Xiaogai Li**, Xingjia Ying*, Marie-Christine Chevalier*, Stefan Kirscht***, Svein Kleiven **

*Univ. Lyon, Ifsttar-Université Claude Bernard Lyon 1, LBMC, UMR_T9406, Bron, France

** Neuronic Engineering, School of Technology and Health, Royal Institute of Technology (KTH), Hälsovägen 11C, 141 57 Huddinge, Sweden, ***Technische Universität Berlin, Department of Automotive Engineering, Gustav-Meyer-Allee 25, 13357 Berlin, Germany

Abstract

Human body Finite element models have the potential to provide significant insight into the paediatric response to impact. However, child models are by far less common and less advanced than their adult counterpart. The aim of the current study is to report on the development of a new child model (PIPER Child model) that aims to be continuously scalable between at least 1.5 and 6 years of age.

After an overview of the model composition for all anatomical regions, examples of simulations performed for its validation are provided for all regions to illustrate the model performance. The scaling methodology used to account for the changes of model dimensions with age is also summarised along with the tool developed to apply the changes (PIPER tools). Short term perspectives include the completion of the validation simulation and the refinement of the scaling procedures to include the effects of age on material parameters, and to develop the capability to scale the model to any external anthropometry target.

The model, along with all validation simulations and associated tool will be released under an Open Source license in April 2017.

Introduction

Human body Finite element models have the potential to provide significant insight into the paediatric response to impact. Because they are not subjected to the same limitations as the physical dummies, they could better describe both variations due to age and size changes as well as responses in multiple directions (omnidirectionality). However, the availability of child human models has been more limited than adults. Also, the data available to verify the response of such models is scarcer than the adult.

In 2015, Beillas *et al.* presented ongoing efforts to upgrade existing human models to better describe the growth process (growth cartilage) and to detail relevant anatomical regions. Regional development efforts were described for the head, neck and shoulder and the application framework was described. However the models were still ongoing heavy development, the regional models were not assembled, the validations of the regional responses were limited and the response of the whole model was not considered. The objectives of this study are to report on the completion of the model development, the status of the validation and provide information regarding the first applications of the model and future public availability.

Methods

Model overview

The main development phase of the PIPER Child human models is now complete (mesh development, material selection, core validation, etc). The baseline model describes a 6 years old (YO) child whose main anthropometric dimensions were normalised by nonlinear scaling (kriging interpolation) using GEBOD (Cheng et al., 1994) regressions as a reference (stature: 1146 mm, seating height: 631mm, etc). Overall, the internal geometry is based on a combination of several CT scans obtained from a children's Hospital under a data sharing agreement (Hospital *HFME*, Hospices Civils de Lyon, Bron, France) for children of different ages (1.5, 3 and 6 YO). Semi-automatic segmentations of the scans were used to define the bony and main organ shapes as well as the evolution of growth cartilage. These were complemented by anatomical descriptions for the placement of ligaments and other structures difficult to see on the scans. The only exception was the foot which was difficult to segment due to the large proportion of growth cartilage and that was derived from the scan of an elderly subject that was scaled to the child size. This was deemed as an acceptable assumption as the foot is still considered as a rigid component. As the scans were performed in a supine position, a postural adjustment of the thoracic and lumbar spine was manually performed by tilting individual vertebrae to approximate the curvature obtained on a seated adult in Upright MRI data (Beillas et al., 2009). The skin was also mostly derived from the CT scans but the postural change required more adjustments: surfaces in different regions (e.g. head, neck, trunk, upper and lower extremities) were assembled in the target posture and the mesh continuity was obtained by interpolation. The trunk skin was deformed to follow the curvature changes. Seated data provided by University of Michigan (OCATD 6YO dataset, and more recently, seated shape based on statistical shape modelling) were used to complement the surface and help with the assembly. While these developments were performed in multiple model iterations (e.g. descriptions in Beillas et al., 2013, 2014a, 2014b, 2015 at the whole body level), the current model version (v0.3) differs very significantly from these previous versions in terms of mesh and description of anatomical structures. It is however in a similar posture (for the spine in particular). An illustration of the geometry of the current version is provided in Figure 1, along with a final shape comparison with UMTRI seated statistical shape model (<http://childshape.org>). Overall, the current model shape is very similar – within a few millimetres – to the UMTRI model for similar anthropometric parameters.

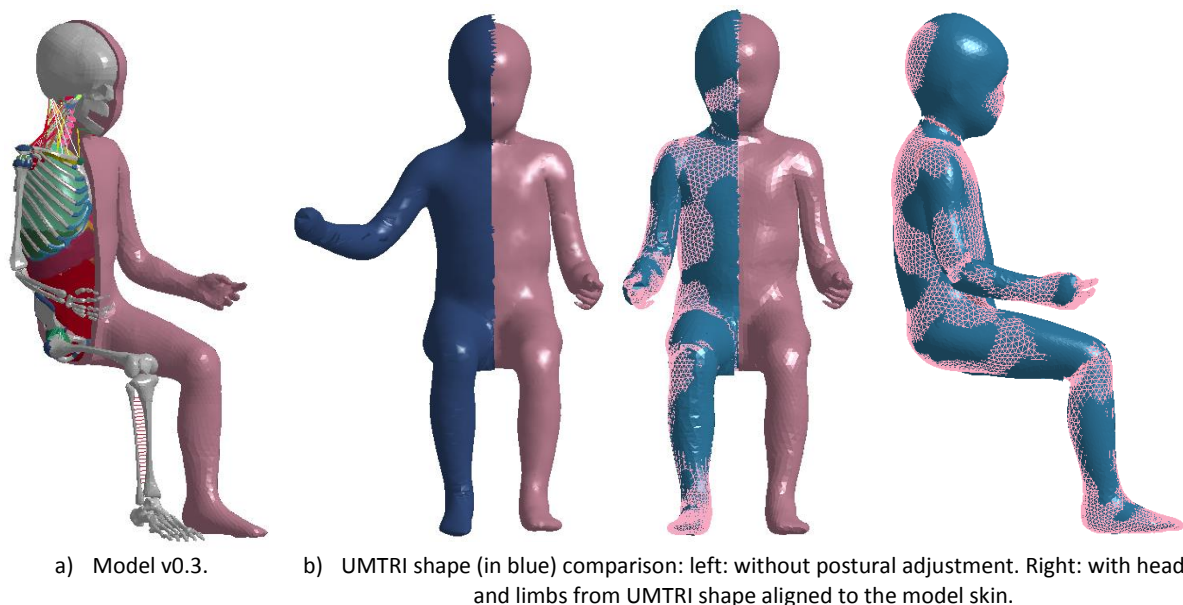


Figure 1 : Overview of the model and comparison with UMTRI seated statistical shape model (parameters: stature 1146 mm, BMI 17.05, SHS: 0.55; recline: 11; Flex: 50; <http://childshape.org>).

In terms of size, the model is comprised of approximately 531,000 elements (including about 52,000 rigid elements) distributed into 353 parts describing the main anatomical structures. The model has a total mass of 23kg (v0.202). It was developed in the Ls-dyna explicit FE code. The model time step is 0.32 μ s with marginal mass scaling (15 grams added). Descriptions of the main anatomical regions, in comparison to previously published versions, will be provided below.

Head

The development of the PIPER head model described in Giordano and Kleiven (2016) was continued. Significant updates were made to the mesh of the brain and meninges with the purpose to improve the quality and stability of the model. According to the human anatomy, the brainstem was described with a cylindrical topology and the thickness of the scalp was adjusted to be on average 5 mm (Loyd 2011). The updated PIPER head model is illustrated in Figure 2. It consists of 26,834 nodes, 41,343 solid elements and 12,764 shell elements and it includes a detailed description of the scalp, the skull, the cerebrum, the cerebellum, the meninges and the cerebrospinal fluid. A typical spatial resolution of 3–5 mm was chosen to capture fundamental anatomical structures but, at the same time, guarantee a reasonable computational time for simulations. The aim of the model is indeed to be robust and scalable, without altering the mesh quality.

A summary of the material properties of the head model is reported in

Table 1. The material properties for the skull bone were taken from Davis et al. (2012) and a linear isotropic elastic constitutive law was used to represent the mechanical properties in the model. The brain tissue was modelled as a nonlinear viscoelastic model described by an Ogden 2nd order constitutive law. According to previous studies (Prange and Margulies 2002, Gefen et al. 2003, Chatelin et al. 2012), at 6 years of age young brain tissue can be considered equivalent to adult tissue.

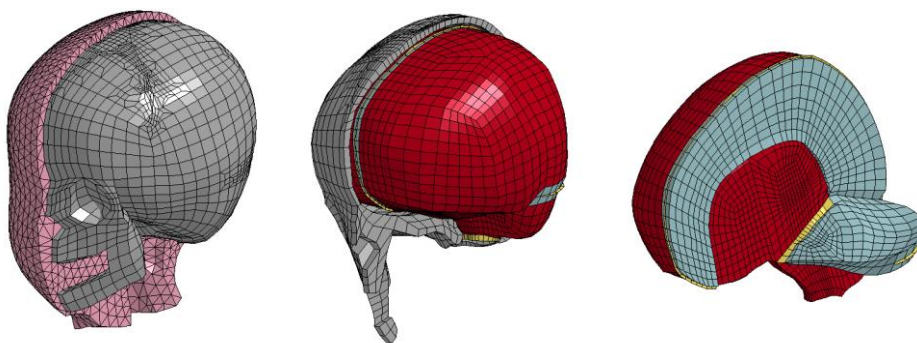


Figure 2: PIPER Child Head Model. From the left to the right: head model with open scalp for visualisation of the skull; head model with open skull for visualisation of the brain; head model with open brain for visualisation of the meninges.

Table 1: Summary of the properties of the 6 YO: Head model components used in this study.

Tissue	Young's Modulus	Density (Kg/m ³)	Poisson's Ratio
Scalp	Ogden 1 st order + viscosity	1140	0.49
Outer Compact Bone	9.0 GPa	2000	0.22
Inner Compact Bone	9.0 GPa	2000	0.22
Porous Bone	1.0 GPa	1300	0.24
Brain Tissue	Ogden 2 nd order + viscosity	1040	~ 0.5
Cerebrospinal Fluid	K = 2.1 GPa	1000	~ 0.5
Dura Mater	Mooney – Rivlin	1130	0.45
Pia Mater	11.5 MPa	1130	0.45
Falx	31.5 MPa	1130	0.45
Tentorium	31.5 MPa	1130	0.45

Neck

The geometry of the vertebrae FE-mesh was based on a CT scan of a 3 YO child, provided by the Hospices Civils de Lyon (HCL, France) and segmented by Ifsttar/UBCL, under a legal agreement allowing the communication of anonymized imaging dataset to help build human models for safety. Using the segmentation, the vertebrae were meshed with hexahedral elements for the cancellous bone and covered with a layer of shell elements to represent the cortical bone. The topology of the mesh was made elliptic to accommodate for a continuous mesh between the vertebrae and intervertebral disks. The topology was also designed to allow for three layers of shell elements to be embedded in the intervertebral disk to represent the annulus fibres, whereas the annulus ground substance was modelled with the surrounding solid elements. In the centre of the disks, the solid elements represented the nucleus pulposus. The typical element size was around 2 mm, needed to capture necessary features of the spine, resulting in 18,396 nodes, 13,276 solid elements, 10,410 shell elements and 828 discrete elements, including ligaments and neck muscles.

The majority of the ligaments were modelled as discrete springs attached according to anatomical descriptions. The exceptions were the vertical cruciate and the transverse ligaments that were modelled with shell elements, needed for the contact between these ligaments and the dens of the second vertebra. The neck muscles were also modelled with discrete elements but were in general split into a number of elements in series in order for them to be constrained to the most adjacent vertebra, which allows for the muscles to bend with the spine under external loading.

The mesh of the 3 YO was scaled to the 6 YO using the PIPER tool, taking into account the development of local features such as facet angles and vertebral height, as described in Beillas et al. (2015). An illustration of the model can be seen in Figure 3. The cortical and cancellous bone was modelled as linear elastic with material properties scaled from adult properties using a scale factor based on bone density from a study by Gilsanz et al. (2009). The annulus ground substance was modelled as a linear viscoelastic, the fibres with linear elastic with two families of fibres and the nucleus pulposus as a linear elastic fluid. The material properties were based on adults and scaled using scaling factors developed in Yoganandan et al. (2000). The ligaments were modelled with nonlinear force displacement curves for adults from (Mattucci et al., 2013; Mattucci and Cronin, 2015), scaled using (Yoganandan et al., 2000). The muscles were modelled with bilinear force displacement curves based on stress-strain properties from (Myers et al. 1995) and cross section area of paediatric neck muscles (Yoganandan et al., 2002).

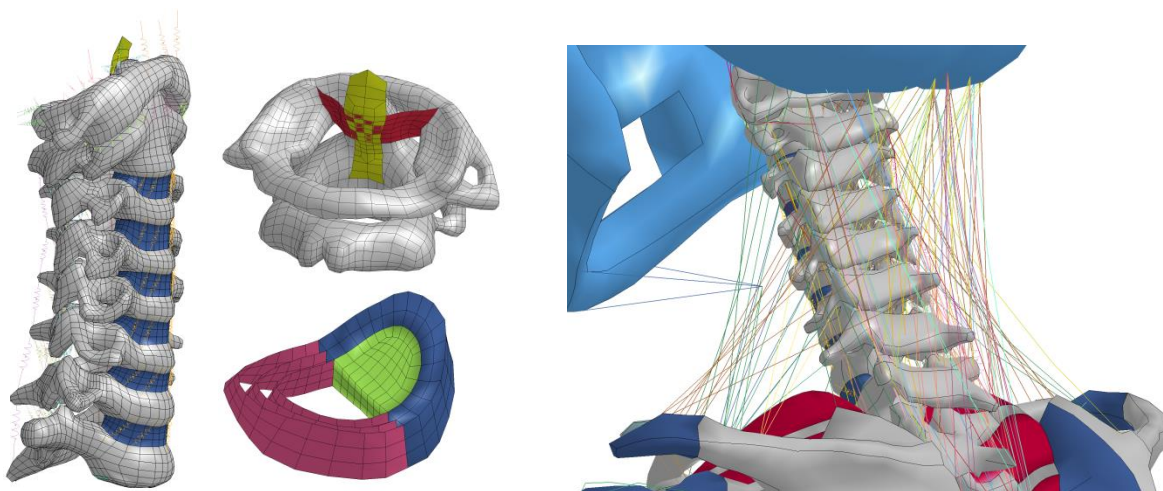


Figure 3. Neck model, visualising the ligamentous spine (left), C1-C2 with shell ligaments (top middle), intervertebral disk (bottom middle) and surrounding muscles with attachment on head, neck and trunk (right).

Table 2: Summary of the properties of the 6 YO neck model.

Tissue	Stiffness	Density (Kg/m ³)	Poisson's Ratio
<i>Cortical bone</i>	E = 12.1 GPa	805	0.29
<i>Trabecular bone</i>	E = 0.4 GPa	242	0.29
<i>Annulus ground substance</i>	K = 2.9 Mpa	3670	--
<i>Annulus fibres</i>	E1 = 23.5 MPa; E2 = 4.4 MPa	3670	v ₁ =0.016; v ₂ =0.45
<i>Nucleus pulposus</i>	K = 1.7 GPa	1000	--

Trunk (thoraco-abdominal and pelvic regions)

While the overall shape of the trunk was kept from Beillas et al, 2015, extensive changes were performed for the soft organs to better describe the anatomical structures and limit the gaps between the organs.

For the skeleton, the pelvis is now meshed with deformable elements (vs. rigid before) describing the cancellous and cortical bone (tetrahedral and shell elements), as well as the growth cartilage (based on the CT). The thoraco-lumbar spine was partially remeshed but remains modelled using rigid vertebrae connected by 6 d.o.f. beams. The ribcage is still described using deformable elements for the ribs, costal cartilage and sternum (solid covered by shells) and connected to the thoracic spine using 6 d.o.f. beams at the costo-vertebral joint. The thoraco-abdominal cavity is separated by the diaphragm which was modified to improve the location of its insertions on the spine and lower ribcage.

For the soft abdomen, muscles of the abdominal wall and retroperitoneal tissues were separated from the former flesh components to provide more accurate anatomical boundaries for the abdominal cavity. For the solid organ, minor changes were performed to smooth their shape and a pancreatic component (corresponding to the pancreas and surrounding fat) was introduced. The small intestines and colon are not separated and are described using an incompressible bag (unchanged). For the thoracic cavity, an incompressible bag formulation is used for the heart, whose geometry was modified to better describe the overall shape of the organ. The lungs remain as compressible bags. In general, non-sliding/attached relationships are described using continuous mesh between parts, while sliding relationships are described with sliding contacts. Illustrations of the model are provided in Figure 4. Properties are derived from the LBMC model (Beillas et al., 2013).

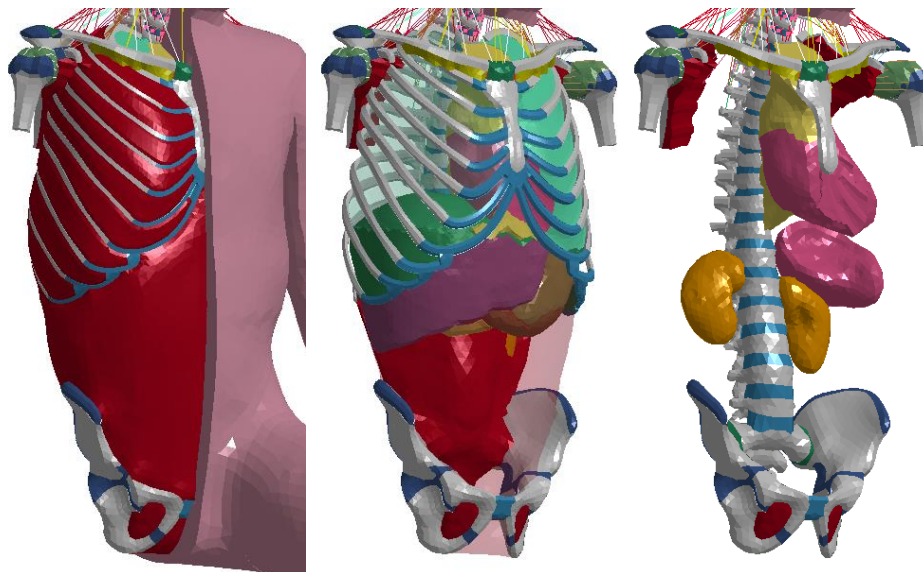


Figure 4. Overview of the trunk (thorax abdomen pelvis) with the skeleton (grey), cartilage (blue). From left to right: skin and flesh removed but abdominal and intercostal muscles visible (red). Center: muscles removed and right lung and hollow organ bags partially transparent to expose the new retroperitoneal component (red). Visible structures include the new diaphragm (green), liver (purple), stomach and pancreatic component (light and dark brown). Right: additional structures are hidden to expose the kidneys, spleen and updated heart.

Upper and lower extremities

The shoulder and upper extremities model are similar to the ones presented in Beillas et al. (2015). It uses deformable elements for the bones and ligaments up to the distal end of the humeral diaphysis. The distal humeral epiphysis, radius and cubitus and hand are modelled as three rigid bodies (one for each) which are articulated at the elbow and the wrist using 6 d.o.f. beams. The scapula can slide over the thorax and sliding contacts are also used for the gleno-humeral and sterno-clavicular joints. An illustration is provided in Figure 5. Properties are mostly derived from the LBMC model.

The lower extremities were largely updated from the previous version. From proximal to distal, the hip is now modelled as a deformable joint (contact between the femoral heads and acetabula, deformable bones and cartilage, capsule and ligaments) as well as the diaphysis of femur, tibia, and fibula (shells located on the mid-cortical surface and variable shell thickness). This was chosen to improve the response in side impact. For the diaphyses, the shell thickness was also adjusted based on the segmentation of the CT-scans and the material properties were modelled first as elastic and then as elastoplastic with required values for the yield stress, ultimate strength and ultimate strain based on Öhman et al., 2011. It was assumed that all stated material parameters are identical in all the three bones.

The distal femur, patella, foot as well as the proximal and distal epiphyses of the tibia and fibula are described using one rigid body each and articulations are provided using 6 d.o.f. beams at the knee and ankle. For the sake of simplicity, the patella is currently linked to the tibial rigid body.

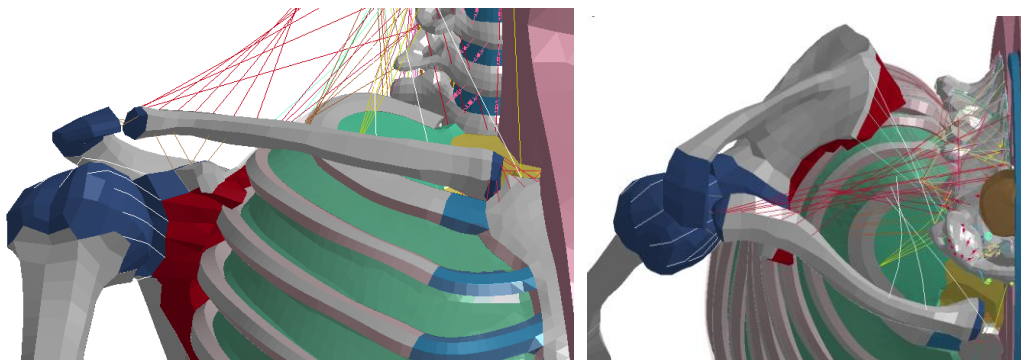


Figure 5. Details of the shoulder model: frontal (left) and top (right) views. The clavicle can slide over the thorax (red surface) and components are deformable (bone in grey, growth cartilage in blue). For clarity, the capsules covering the joints (sterno-clavicular, gleno-humeral, ...) are not shown. Discrete or beam element are used to describe the ligaments and neck muscle.

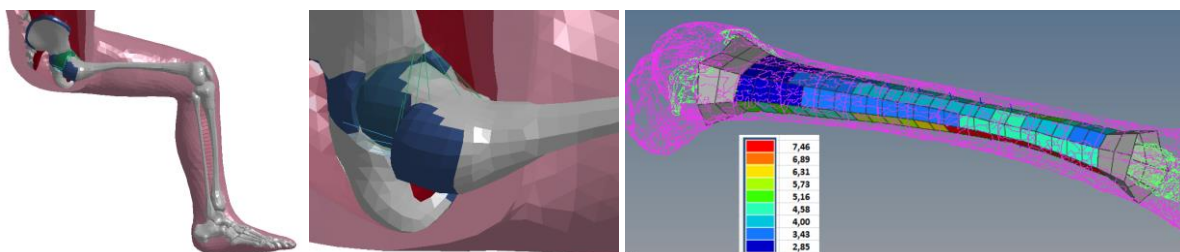


Figure 6. Model of the lower extremity. All bones are now described but only the hip and femoral diaphysis are simulated with deformable components. The shell thickness distribution of the femoral diaphysis is also shown (in mm).

Metadata and PIPER tool integration: age scaling and positioning

Parallel efforts are ongoing in the PIPER project to develop software tools to position and personalise human body models (PIPER software framework, www.piper-project.eu). The child model has been used as one of the development platforms for the tools. As such, positioning and scaling applications are already available in the development version of the software. While it is not the aim of this study to describe the tool, illustrations of the current integration will be shown.

For scaling, previous work performed on scaling based on anthropometric dimensions from GEBOD was further developed and integrated into the database. In this approach, regressions based on GEBOD are used to compute anthropometric dimensions which are represented by a network of carefully selected control points. The control points are then used to drive the model morphing (nonlinear interpolation by Kriging). The regressions can be calculated between 6 and 1.5 years old (using extrapolation between 2 and 1.5 years old). As these dimensions do not provide information about local changes, additional constraints were added to the head and neck region and may be also added to other regions in the future. For the neck, control points help drive the change of local features such as the angle of the facette joints. Similarly, in order to account for variations in head segments proportions with age, the head control point network is based on anatomical landmarks (glabella, opistocranium, tragus, vertex, nasion and mental protuberance) and the dimensions are taken from the Snyder et al. 1977 database. Illustrations of the control points will be provided in the result section.

For positioning, the whole body structure is described using a metadata system allowing the importation of the model and its use in a real-time pre-positioning system based. The pre-position can then be used to update the model mesh or exported to serve as a basis for a full positioning simulation.

Model validation

The targeted validation matrix was compiled based on various literature sources, prioritising data collected on paediatric PMHS and aiming to cover both frontal and side impact. Some setups were also included to allow for comparisons with the dummies. Its backbone is composed of the validation setups used for the previous LBMC model (Beillas et al., 2013) and the head validation setups (Giordano et al, 2016), with addition for neck response, femoral diaphysis and side impact.

As the model is evolving rapidly, not all simulations could be re-run on the exact same version of the model but it is reasonable to expect that the version differences would not affect the response. The successive versions include models with updated trunk (0.202), head and neck (0.3), and femoral diaphysis (0.301). Also, as scaling efforts and integration in the PIPER tool are evolving quickly, the validation could not cover all ages yet and the runability of the derived models remains to be checked.

A summary of the validation status is provided in Table 2. Some of the simulations available for the current versions were run without issue or significant mismatch on previous versions and need to be repeated. It is aimed to perform at least the sets 1 and 2, and perhaps some of the set 3 prior to the public release of the model.

Table 2 : Configurations considered for the model validation and validation status. Set 1 was selected to cover the main regions, mostly at the 6 YO age and is almost completed on current versions. Set 2 correspond to planned configurations (mainly covering other ages or loading mechanisms). Set 3 corresponds to situations that may or may not be simulated (not matching configurations or ages, redundant). *= with a previous version of the model. Need to be updated.

Set	Published Study	ROI	Dir	Impactor/loading	Subjects and ages	Target model and version		
1	Loyd (2011)	Head		Drop test (dyn)	PMHS	9	6	0.3
	Loyd (2011)	Head		Compression (dyn)	PMHS	9	6	0.3
	Ouyang et al. (2005)	Neck		Bending+tensile	PMHS	6	6	0.3
	Ouyang et al. (2005)	Neck		Bending+tensile	PMHS	3	3	0.3
	EEVC Q (2008)	Shoulder	Side	Pendulum, free back (dyn) Scaled	PMHS	Adult	6	0.202
	Ouyang et al (2006)	Thorax	Frontal	Pendulum, free back (dyn)	PMHS	6+	6	0.202
	Kent et al (2011)	Thorax	Frontal	Belt distributed, fixed back (dyn)	PMHS	6 & 7	6	0.202
	Kent et al (2011)	Thorax	Frontal	Belt diagonal, fixed back (dyn)	PMHS	6 & 7	6	0.202
	EEVC Q (2008)	Abdo	Frontal	Belt, fixed back Scaled corr.	Porcine	6	6	0.202
	Kent et al (2011)	Abdo	Frontal	Belt mid abdo, fixed back (dyn)	PMHS	6 & 7	6	0.202
	Kent et al (2011)	Abdo	Frontal	Belt upper abdo, fixed back	PMHS	6 & 7	6	0.202
	Part 572	Lumbar	Frontal	Torso flexion (static)	HIII	6	6	0.202
	Ouyang et al (2003a)	Pelvis	Side	Pendulum, free back (dyn)	PMHS	various	6	0.202
	Ouyang et al. (2003b)	Femur		Bending test	PMHS			0.301
	Wismans et al (1979)	WB neck	Frontal	Sled test, harness (4 YO anthro)	PMHS	6	6	0.3
	Kallieris et al (1976)	WB	Frontal	Sled test with shield	PMHS	2.5, 6		*
	Lopez et al (2011)	WB spine	Frontal	Sled test with belt (dyn)	Volunteer		6	*
	Arbogast et al (2009)	WB neck	Frontal	Sled test, 3pt belt	Volunteer	6+	6	*
2	EEVC Q (2008)	Shoulder	Side	Pendulum, free back (dyn) Scaled	PMHS	Adult	3	*
	EEVC Q (2008)	Shoulder	Side	Pendulum, free back (dyn) Scaled	PMHS	Adult	1.5	planned
	Loyd (2011)	Head		Drop test (dyn)	PMHS	1.5	1.5	0.202
	Loyd (2011)	Head		Drop test (dyn)	PMHS	1	1	0.202
	Loyd (2011)	Head		Compression (dyn)	PMHS	1	1	0.202
	Luck et al. (2008)	Neck		Tensile	PMHS	1.5	1.5	planned
	Luck et al. (2012)	Neck		Tensile segments	PMHS	1.5, 6	1.5, 6	planned
	Luck et al. (2012)	Neck		Bending segments	PMHS	1.5, 6	1.5, 6	planned
	Ouyang et al (2006)	Thorax	Frontal	Pendulum, free back (dyn)	PMHS	2-5	1.5	*
	Ouyang et al (2006)	Thorax	Frontal	Pendulum, free back (dyn)	PMHS	2-5	3	*
Chamouard (1996)	Thigh	Vertical	Belt compression (static)	Volunteer		6	*	
3	Davidson et al (2013)	Shoulder	Frontal	Arm pull, shoulder mobility	Volunteer	Adult		planned
	Kent et al (2011)	Abdo	Frontal	Belt lower abdo (dyn)	PMHS	6 & 7	6	*
	EEVC Q (2008)	Abdo	Frontal	Belt, fixed back Scaled corr.	Porcine	1.5	1.5	
	EEVC Q (2008)	Abdo	Frontal	Belt, fixed back Scaled corr.	Porcine	3	3	
	Kent et al (2008)	Abdo	Frontal	Belt, fixed back (dyn)	Porcine	6	6	*
	Ouyang et al (2006)	Abdo	Frontal	Pendulum, free back (dyn)	PMHS	2-5	1.5	
	Ouyang et al (2006)	Abdo	Frontal	Pendulum, free back (dyn)	PMHS	2-5	3	
	Ouyang et al (2006)	Abdo	Frontal	Pendulum, free back (dyn)	PMHS	6-?	6	
	Chamouard (1996)	Abdo	Frontal	Belt compression (static)	Volunteer		6	*
	Seacrist (2014)	WB	Oblique	Sled test (dyn)	Volunteer	6-8	6	
Ita et al (2014)	WB	Lateral	Shoulder test	Volunteer	4-7	6		

Results

Integration into the PIPER tool: dimension (Age) scaling and positioning

The scaling driven by the relationships between age and dimensions was initially developed as a standalone script (Scilab first, then Matlab/octave). It is now fully integrated into the PIPER tool (Figure 7). This allows deforming interactively the model to any age/stature in the range 1.5-6 y.o. and then saving it for a simulation (Figure 8). The quality of the hexahedral mesh of the deformed models is reported in Table 3 for the 5, 4, 3 and 2 y.o. child models. A comparison with the original mesh is provided.

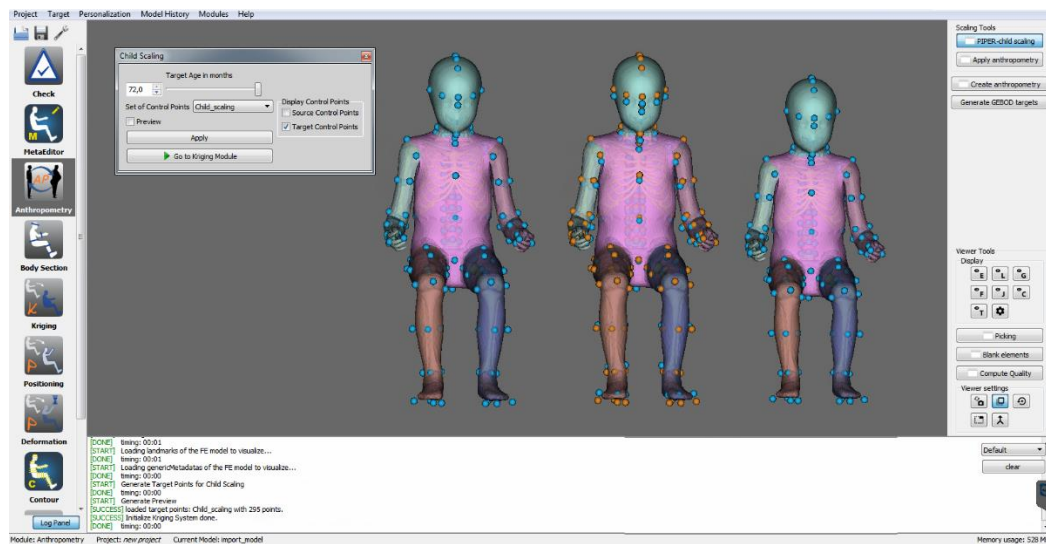


Figure 7: Child model in the PIPER tool. From left to right: network of control points defined on the 6YO model, control points and their target defined corresponding to the 5YO dimension, model deformed to the 5YO child. The target age is simply selected by the user using a slider (left) and the model scaling takes only a few seconds. The PIPER tool has its own 3D viewer to display FE models.

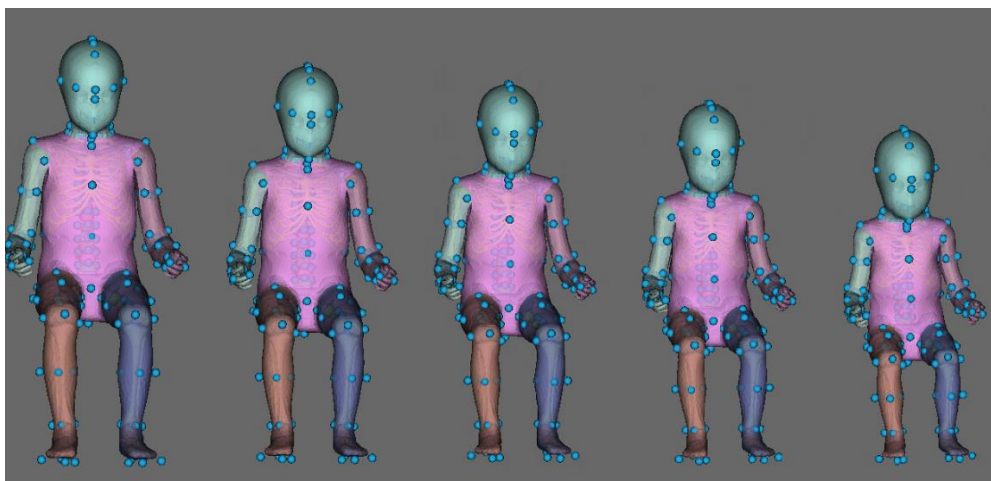


Figure 8: Child model in the PIPER tool. The model is displayed together with the network of control points used for deformation (target points). From the left to the right: 6YO child model (baseline), 5YO, 4YO, 3YO and 2YO child models (derived by Kriging).

Table 3: Quality of the hexahedral mesh of the baseline model (6y.o.); comparison to models deformed by Kriging in the PIPER tool.

Quality	Allowable	Min or Max Value					Violated (%)				
		6yo	5yo	4yo	3yo	2yo	6yo	5yo	4yo	3yo	2yo
Jacobian	> 0.3	0.23	0.23	0.23	0.22	-0.14	5e-4	5e-4	5e-4	5e-4	5e-4
Aspect Ratio	< 8	13.28	13.43	13.57	13.72	14.12	9e-4	1e-3	1e-3	2e-3	2e-3
Min Side Length	> 1 mm	0.33	0.28	0.25	0.21	0.15	5	6	6	6	6
Warpage	< 50°	93.7°	97.1°	100°	103.3°	179°	9e-4	8e-4	7e-4	8e-4	9e-4
Min Quad Angle	> 15°	15°	15°	14.9°	14.8°	13.4°	0	0	0	0	0
Max Quad Angle	< 165°	165°	165°	164°	163.7°	343°	0	0	0	0	6e-4

As it can be seen from Table 3, for most of the quality metrics the Kriging deformation did not significantly affect the quality of the mesh (with exception of ages <3y.o.). Not surprisingly, as the global dimensions of the models increased with age, the most affected metrics were the aspect ratio (decreasing with age) and the minimum side length (increasing with age). Overall, the deformed mesh showed very similar quality with respect to the deformed mesh. For lower ages (<3y.o.), some distortions occurred in the C6 vertebrae of the neck model (Figure 9, less than 5 elements involved), which explain the degraded minimum/maximum value of the Jacobian, warpage angle and maximum quad angle. More work is therefore necessary to adjust the local network of points before the release of the model and prevent this kind of distortions.

The runability of the deformed models was tested in chest impacts with the set-up described by Ouyang et al. 2006. The scaled tested up to now appear to be runnable (Figure 10) and some were used for the validation work.

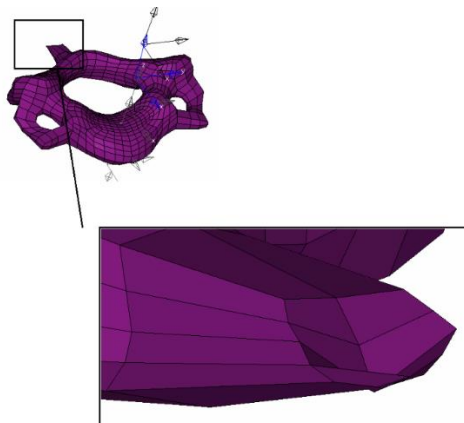


Figure 9: Mesh distortions in the deformed 2 y.o. model. The Jacobian is inverted in four elements of the sixth vertebrae of the cervical spine.

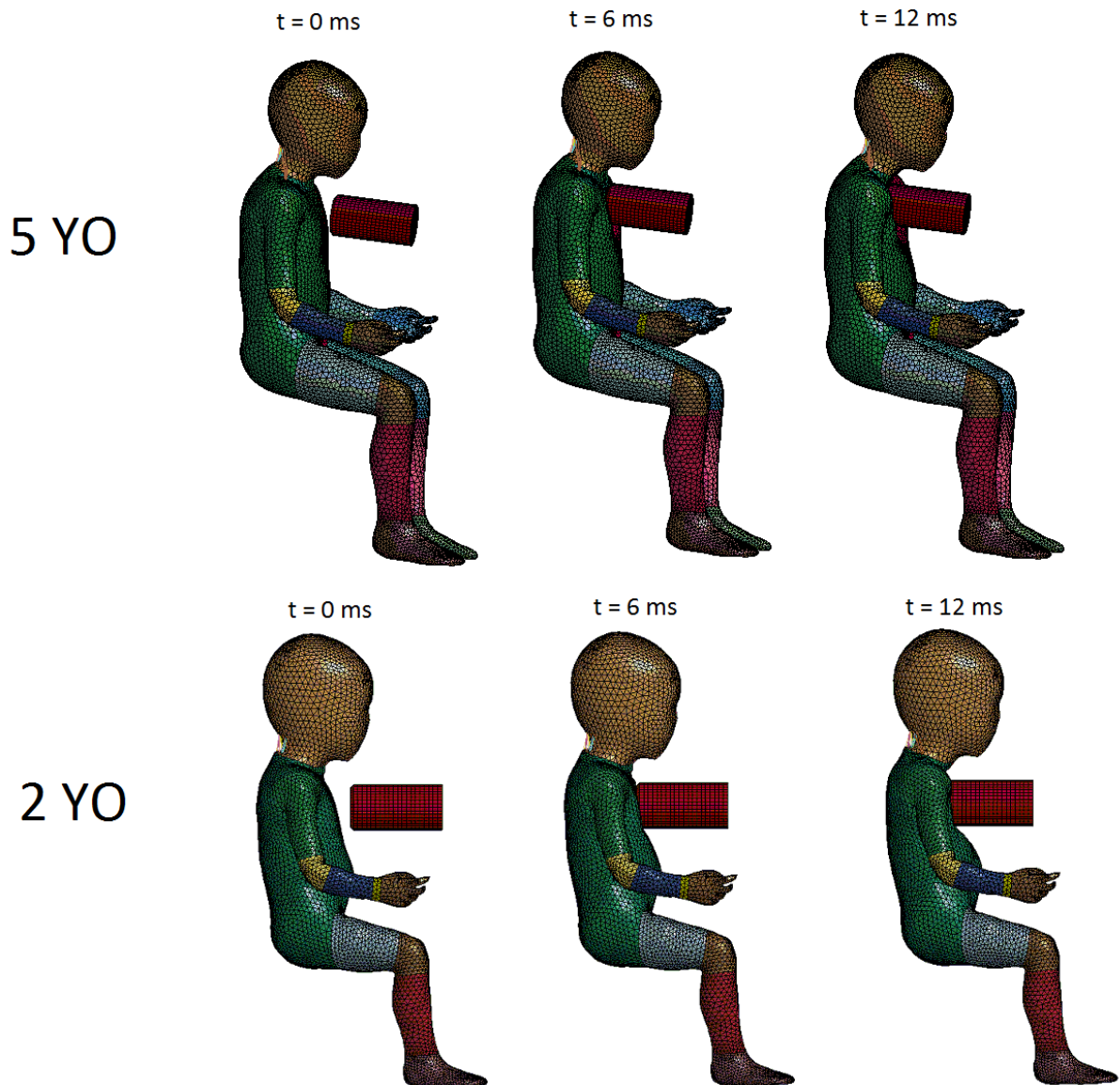


Figure 10: Test for checking the capability of the deformed models to run. On the top: chest impact for the 5 YO model obtained from PIPER tool. On the bottom: chest impact for the 2 YO model obtained from PIPER tool (the negative Jacobians observed in a few elements were manually corrected but will be prevented before the final release).

An illustration of the work ongoing on model positioning is provided in Figure 11. The metadata describing anatomical entities allow to pre-position interactively the model in real time. The model can then be transformed (geometrically, without FE simulation) and the transformation can be smoothed to try to prevent negative volumes. The transformed model could also be used as a target for a full FE positioning simulation.

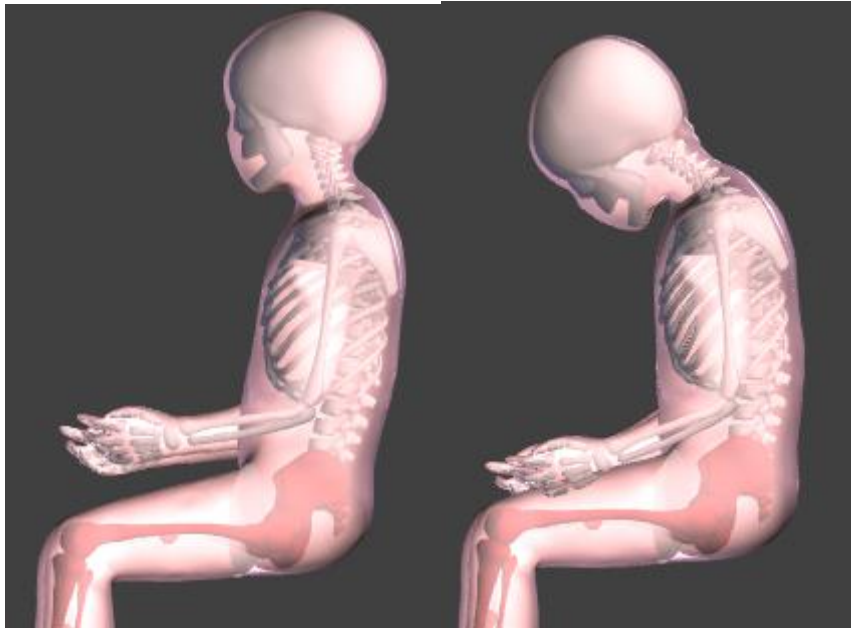


Figure 11: Positioning process: the metadata defined on the child model allow to perform interactive pre-positioning in real time to prepare the model transformation

Validation

The new model appeared to be stable in the configurations that were run. A few examples from the matrix detailed in Table 1 are provided below for each region, with brief descriptions of the simulation setups.

Head

The validation matrix included non-destructive drop tests and compression tests from Loyd (2011). These tests were conducted to check the kinematics and the global properties of the head model, such as the structural stiffness and the distribution of masses. Data referring to P18M (6 YO head model), P17F (1.5 YO head model) and P15F (1 YO head model) was used as experimental target for the simulations. For the drop tests, the head was dropped from heights of 15 and 30 cm onto five different impact locations: vertex, occiput, forehead, left parietal, right parietal. The impact occurred with a smooth flat aluminium plate and the resultant acceleration of the head was measured. For the compression tests, the head was compressed in the lateral and anterior-posterior directions a constant normalised displacement rate test of 0.3/s. The force-deflection curves were measured. For the simulations, the 1.5 YO scaled model (was obtained from the 6 YO using the PIPER tool and Kriging as previously described. Material properties were also adapted to match features of a 1.5 YO child according to the method described in Giordano and Kleiven (2016). The 1 YO child model was generated aside of PIPER tool, with a standalone script, by targeting the anthropometric dimensions of the P15F PHMS.

Figure 12 shows the comparison between the experimental and simulated head resultant acceleration for a selection of the drop tests. The model responses were typically in agreement with the experimental data. Further validation of the model is provided in Figure 13, where a comparison between simulated and experimental response to a selection of the performed low-rate compression tests is shown. The model response was again in agreement with the experimental data.

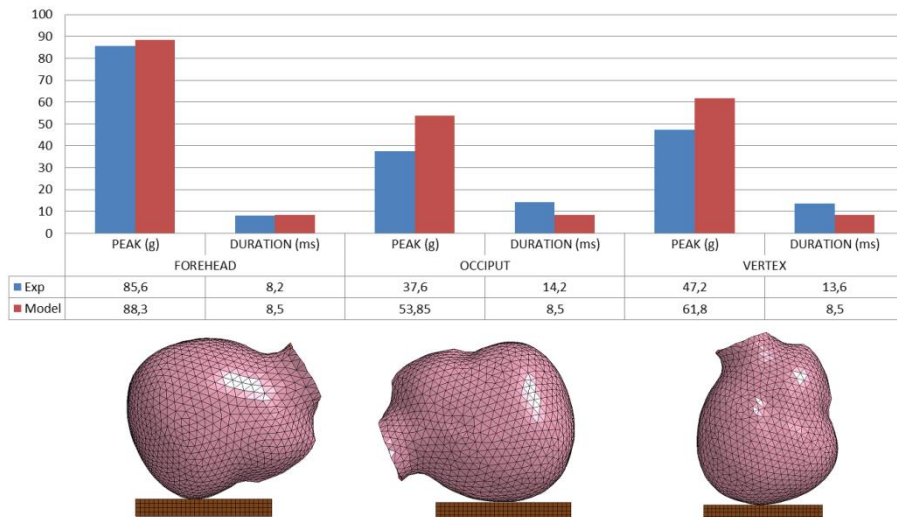


Figure 12: Summary of the drop test results for the 1.5 YO model. On the top: comparison between experimental (blue) and simulated responses (red). On the bottom: set-up of the drop tests. The head was dropped from a height of 15 to an aluminium plate onto three locations.

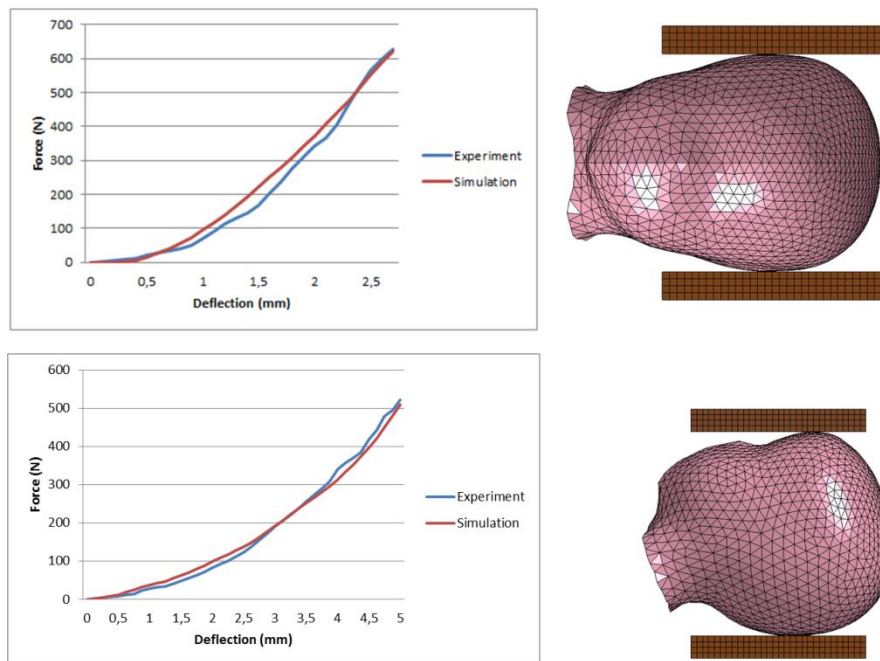


Figure 13: Summary of the compression tests. On the top: comparison between experimental (blue) and simulated responses (red) for 0.3/s lateral compression of the 6 YO head model. On the bottom: comparison between experimental (blue) and simulated responses (red) for 0.3/s anterior-posterior compression of the 1 YO head model

Neck

For the neck, the simulation results corresponding to the bending tests performed by Ouyang et al. (2005) are provided in Figure 14. These tests allow characterising the overall stiffness of the cervical spine in flexion and extension. The model response was found to be within the range of the PMHS results. However, since the results are only available for a limited number of specimens of different ages and that no clear trend can be observed between age and response, it is difficult to further refine the comparison.

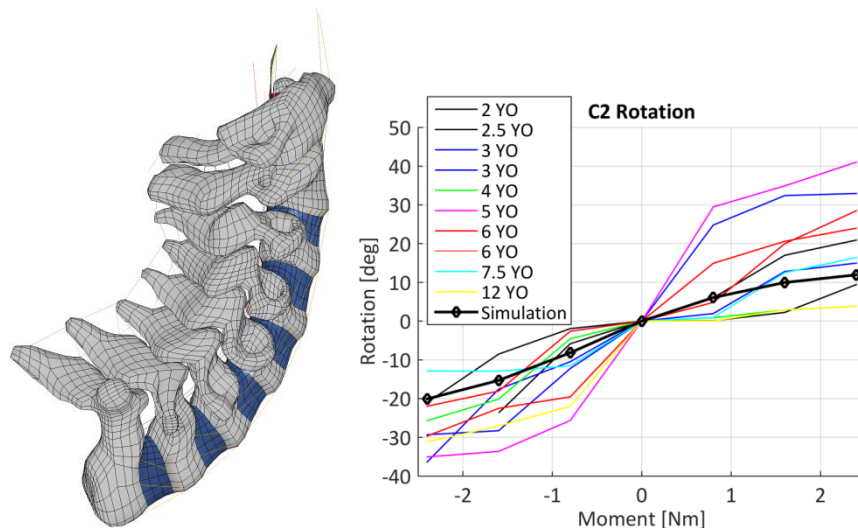


Figure 14: Neck simulations corresponding to Ouyang et al. 2005. Left: bending at 24N.m. Right: simulation results for 8, 16 and 24 Nm compared with the PMHS tests

Trunk

First, simulations were rerun to see if the changes performed in terms of internal anatomy had affected the response in comparison with the LBMC model (Beillas et al., 2013). While difference can be observed, they are relatively small and still seem acceptable considering the typical subject to subject variability. An example of these simulations (Kent et al., 2009, 2011) is provided in Figure 15. In that case, differences may be due to the change of model for the heart and surrounding tissues.

For side impact, an illustration of the response for the shoulder impact (scaled corridor) is provided in Figure 16. The shoulder force and peak deflection are close to the corridor but slightly above the upper bound. The reason for these differences is unknown but the fact both force and deflection are overestimated could suggest that the stiffness of the region is not the issue. While this should be further investigated to understand which parameters could affect these peaks, these results could be considered acceptable for now considering the response of the current dummy (e.g. Q6) and the fact that the corridors are not obtained on paediatric PMHS but derived by scaling.

Also for side impact, the 6 YO model response was compared to the pelvic side impact tests published by Ouyang et al (2003a). In these tests, the impact is delivered on the pelvis using an impactor with a flat surface covered with sorbothane while the opposing side is against a fixed support covered with neoprene foam. The force vs. impact displacement experimental curves include a loading phase that is almost linear until a peak or plateau is reached, which is followed a reduction of the force while the impactor displacement continues. After simulating the test setup (including the polyurethane), the main trends of the curves were captured by the model (almost linear force increase until a peak, followed by a continued displacement at a decreased force). However, while the peak force was captured, it occurred later in the simulation than in the tests and the total impactor displacement was more limited. A plateau visible on the simulated impactor force around 10 to 20 mm could be responsible for some of these discrepancies but its cause is unknown. As many factors could affect this response (anthropometric differences, pelvic translation and compression of the contra lateral tissues, etc), a preliminary sensitivity analysis was performed. Up to now, none of the parameters tested (e.g. reduced soft tissue thickness on the impactor side, increased abdominal bag mass, increased pelvic cartilage stiffness) had an effect that could explain the discrepancies between simulations and tests.

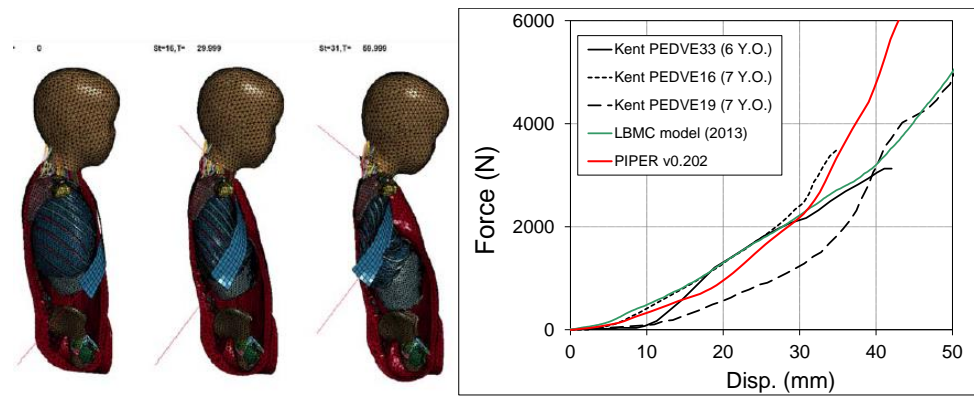


Figure 15: Simulation of the response for the diagonal belt compression (tests from Kent et al, 2009, 2011). Left: illustrations for the updated model (v0.202). Right: responses of LBMC model (in green) and the updated model (in red). While differences can be seen on the response curves, they remain within the range of results observed on the three PMHS.

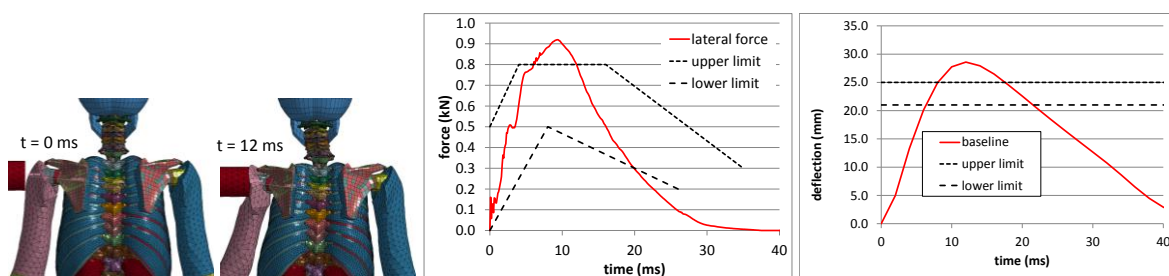


Figure 16 : Shoulder impact (6YO corridors, rigid impactor mass=2.9 kg - v =4.5 m/s). Left: illustrations for the updated model. Right: response curves

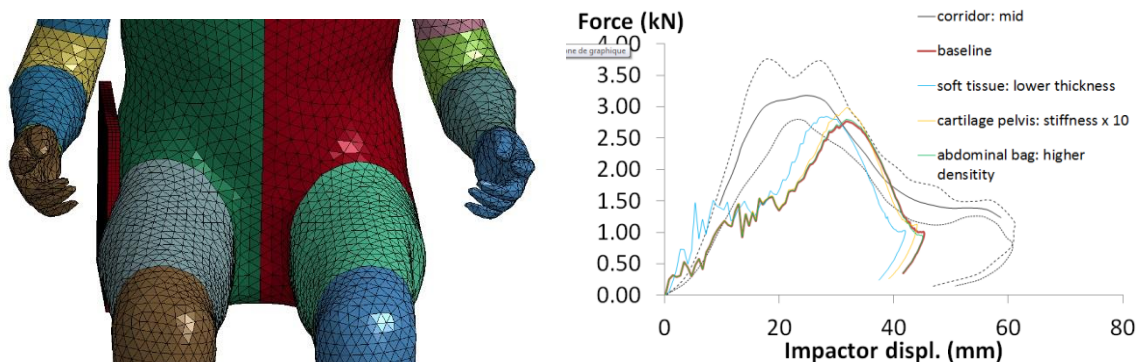


Figure 17: Pelvic impact (Ouyang et al., 2003). Left impact setup showing the contralateral support plate. Right: impact response for various simulation parameters.

Lower extremity

The bending behaviour of the lower extremity long bones was compared to data published by Ouyang et al. (2003b). In these study, three-point-bending test were conducted. The corresponding results show relatively large subject to subject variations for subjects aged between 5-7 years (n=5). While static and dynamic loading were both tested for the femur, tibia and fibula models, the dynamic loading condition was considered more valuable for the current application. The comparison of the model response and the failure points published by Ouyang et al. is provided in Figure 18. The model responses are overall in agreement with the experimental results up to failure levels for the femur and fibula. Failure seemed to occur later in the simulation than the experiments for the tibia. No further adjustment was performed for now however.

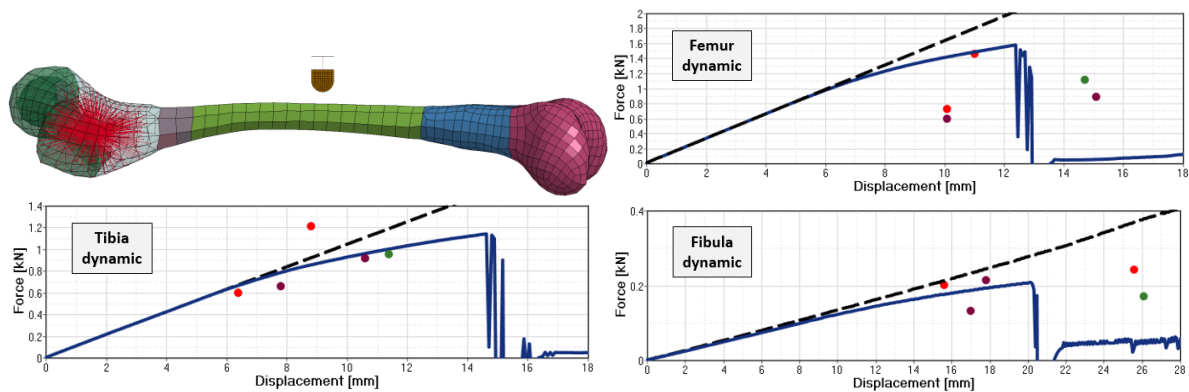


Figure18. Comparison of the model responses with the Ouyang et al. (2003) diaphysis bending results. Top left: simulation setup for the femur. Other: simulation results for femur, tibia and fibula in dynamic bending with elastic (dashed) and elastoplastic (solid) material definition compared to results for 5-7 years-old specimens (dots).

Whole body response

The runs to check the response of the assembled model (v0.3) in sled configuration are ongoing. As a first illustration, a simulation for the Wismans et al (1979) sled test with harness is shown in Figure19. Results seem overall in line with the LBMC model (2013) and other runs performed with that model will now be repeated (Kallieris et al, 1976, Arbogast et al., 2009, Lopez et al, 2011).



Figure19: Sled test with harness from Wismans et al. (1979): illustration of the model response.

Discussion and conclusions

The work on a continuously scalable full body model of a child has continued in the PIPER project. The model mesh is now completed, and comparisons with experimental references were performed in all body regions (“validation” process). The results are very encouraging with generally a good match between the model response and the reference. Some discrepancies – which are not believed to be major – are visible in some cases. For these, sensitivity analyses are ongoing to try to understand if the difference could be due to erroneous assumptions, to the fact that it is not possible to capture the full experimental variance with a single model, or to some of the scaling assumptions used for the reference. The work will continue on this validation process to extend the comparisons to more references as outlined in Table 1. It is not expected that the model will be able to match all sources of data, but the process will allow understanding how the model is positioned with respect to the current biomechanical knowledge.

Concerning the scaling, the size dependency to the age was refined, and a scaling process was integrated into the PIPER tool. This allows a completely interactive and user-friendly scaling to average anthropometry targets based on GEBOD as a function of age. Work on this activity will continue by refinement of the anthropometric target and elimination of the mesh distortions. Also,

work is ongoing to include the dependency of material properties (brain, growth cartilage reduction...) to the age in the PIPER tool.

Another short term perspective is the scaling of the model using other sources than GEBOD. A method (Parkinson and Reed, 2010) allowing to predict a set of anthropometric dimensions based on arbitrary predictors (e.g. age, BMI, stature, arm length) was implemented in the PIPER tool and applied to the adult using the ANSUR database. The implementation using the Snyder et al (1977) public database of child anthropometric dimensions is ongoing. This should allow driving the child model scaling by any set of anthropometric dimensions, and in particular, generating models that describe the bounds (e.g. in terms of shoulder width) described in the R129 regulation. Other applications (including some accident reconstructions, repositioning with the PIPER tool) will be performed in the next few months. Future work (beyond PIPER) will include work to estimate injury tolerance levels.

The PIPER child model, its complete set of validation setups, its metadata for use with the PIPER tool, and the PIPER tool itself will all be publicly released under an Open Source license in April 2017. For the tools, a standard GPL license will be used (V2). For the child model, the GPL version 3 license will be used, with additional clauses requesting to publish model modification any time a publication using the model is published. Altogether, this should provide an Open, easy to use environment for child simulation and should promote the reproducibility of modelling studies.

Acknowledgements

This research has received funding from the European Union Seventh Framework Program ([FP7/2007-2013]) under grant agreement n°605544 [PIPER project]). More information about the project, partners, ongoing activities, roadmap and model release can be found at www.piper-project.eu.

References

- Arbogast KB, Balasubramanian S, et al. (2009) Comparison of kinematic responses of the head and spine for children and adults in low-speed frontal sled tests. *Stapp Car Crash J*, 53:329-372.
- Beillas, P., Lafon Y., and Smith F.W. (2009) The Effects of Posture and Subject-to-Subject Variations on the Position, Shape and Volume of Abdominal and Thoracic Organs. *Stapp Car Crash Journal* 53:127–54.
- Beillas P., Soni A., Renaudin F., Johannsen H. (2013) Comparison of the submarining behaviors of a 6 years old human model and a Q6 dummy in sled testing. 11th Conference on the Protection of Children in Cars, Munich, Dec 5, 2013
- Beillas P., Soni A., Chevalier M-C., Johannsen H., Müller G., Holtz J., (2014a) Q6 Dummy Thoracic Response and Diagonal Belt Interactions: Observations based on Dummy Testing and Human and Dummy Simulations, IRCOBI Conference Proceeding. Paper IRC-14-39. Berlin, 2014.
- Beillas P., Soni A. (2014b) Assessment of abdominal loading by shield CRS in frontal impact: comparison between direct loading in isolated tests and sleds. 12th Conference on the Protection of Children in Cars, Munich, Dec 4-5, 2014
- Beillas P., Giordano C., Alvarez V., Collot J., Kirscht S., Kleiven S (2015) Ongoing efforts on scalable child models, associated tools and procedures in the PIPER project. 13th International Conference Protection of Children in Cars. Dec 3-4, Munich. Germany
- Chamouard F., Tarrière C, Baudrit P. (1996) Protection of children on board vehicles: Influence of pelvis design and thigh and abdomen stiffness on the submarining Risk for dummies installed on a booster. ESV Paper Number 96-S7-O-03

- Chatelin S, Vappou J, Roth S, Raul JS, Willinger R. Towards child versus adult brain mechanical properties. *Journal of Mechanical Behavior of Biomedical Materials*, 2012, 6: 166-173.
- Cheng H., Obergefell L., Rizer A., "Generator of Body Data (GEBOD) manual", Report No.AL/CF-TR-1994-0051. Human effectiveness Directorate, Crew Survivability and Logistics Division, Write-Patterson Air Force Base, Ohio, 1994.
- Davis MT, Loyd AM, Shen HH, Mulroy MH, Nightingale RW, Myers BS, Bass CD. The mechanical and morphological properties of 6 year-old cranial bone. *Journal of Biomechanics*, 2012, 45: 2493-2498.
- Gefen A, Gefen N, Zhu Q, Raghupathi R, Margulies S. Age-Dependent Changes in Material Properties of the Brain and Braincase of the Rat. *Journal of Neurotrauma*, 2003, 20(11): 1163-1177.
- Gilsanz, V., Perez, F. J., Campbell, P. P., Dorey, F. J., Lee, D. C., & Wren, T. a L. (2009). Quantitative CT Reference Values for Vertebral Trabecular Bone Density in Children and Young Adults, 250(1)
- Giordano C, Kleiven S. (2016). Development of a 3-year-old Child FE Head Model, Continuously Scalable from 1.5- to 6-year-old. Proceedings of the IRCOBI Conference 2016, Malaga, Spain.
- Irwin A.L., Mertz H.J., Elhagediab A.M. and Moss S. (2002) Guidelines for Assessing the Biofidelity of Side Impact Dummies of Various Sizes and Ages. *Stapp Car Crash Journal*, Vol. 46 (November 2002)
- Ita, Meagan, Yun-Seok Kang, Thomas Seacrist, Eric Dahle, and John Bolte IV. (2014) Comparison of Q3s ATD Biomechanical Responses to Pediatric Volunteers. *Traffic Injury Prevention* 15, no. sup1 (September 26, 2014): S215–22.
- Kallieris D, Barz J, Schmidt G, Hess G, Mattern R. (1976) Comparison between child cadavers and child dummy by using child restraint systems in simulated collisions. *Stapp Car Crash Conference*, paper 760815, Dearborn, MI, USA.
- Kent R, Salzar R, Kerrigan J, et al. Pediatric thoracoabdominal biomechanics. *Stapp Car Crash J*, 2009, 53:373-401.
- Kent R, Lopez-Valdes FJ, et al. Characterization of the pediatric chest and abdomen using three post-mortem human subjects. *Proceedings of the 22nd ESV Conference*, 2011, Washington DC.
- Loyd AM. Studies of the Human Head From Neonate to Adult: An Inertial, Geometrical and Structural Analysis with Comparisons to the ATD Head. Dissertation. Department of Biomedical Engineering, Duke University, 2011.
- Luck, J.F., (2012). The Biomechanics of the Perinatal, Neonatal and Pediatric Cervical Spine: Investigation of the Tensile, Bending and Viscoelastic Response. Duke University.
- Mattucci, S. F. E., & Cronin, D. S. (2015). A method to characterize average cervical spine ligament response based on raw data sets for implementation into injury biomechanics models. *Journal of the Mechanical Behavior of Biomedical Materials*, 41, 251–260.
- Mattucci, S. F. E., Moulton, J. a., Chandrashekar, N., & Cronin, D. S. (2013). Strain rate dependent properties of human craniovertebral ligaments. *Journal of the Mechanical Behavior of Biomedical Materials*, 23, 71–79.
- Myers, B., Van Ee, C., Camacho, D. L. A., Woolley, T., & Best, T. (1995). On the structural and material properties of mammalian skeletal muscle and its relevance to human cervical impact dynamics. *SAE Technical Paper*.
- Öhman C, Baleani M, Pani C, Taddei F, Alberghini M, Viceconti M, Manfrini M. Compressive behaviour of child and adult cortical bone. *Bone*, 2011, 49(4): 769-776)
- Ouyang J, Zhu QA, Zhao WD, Xu YQ, Chen WS, Zhong SZ., 2003a. Experimental cadaveric study of lateral impact of the pelvis in children, *Academic Journal of the First Medical College of PLA*, 2003a, 23(5), 397-401, 408

- Ouyang J, Zhu QA, Zhao WD, Xu YQ, Chen WS, Zhong SZ., 2003b. Biomechanical Character of Extremity Long Bones in Children and its Significance. *Chinese Journal of Clinical Anatomy*, 21: 620-623
- Ouyang, J., Zhu, Q., Zhao, W., Xu, Y., Chen, W., & Zhong, S., 2005. Biomechanical Assessment of the Pediatric Cervical Spine Under Bending and Tensile Loading. *Spine* 30.
- Ouyang, J., Zhao, W., Xu, Y., Chen, W., & Zhong, S. (2006). Thoracic impact testing of pediatric cadaveric subjects. *The Journal of Trauma*, 61(6), 1492-1500.
- Parkinson, M. and Reed, M.P. (2010). Creating virtual user populations by analysis of anthropometric data. *International Journal of Industrial Ergonomics* 40, 106–111
- Prange M, Margulies S. Regional, directional, and age-dependent properties of brain undergoing large deformation. *Journal of Biomechanical Engineering*, 2002, 124: 244–252.
- Seacrist, Thomas, Caitlin M. Locey, Emily A. Mathews, Dakota L. Jones, Sriram Balasubramanian, Matthew R. Maltese, and Kristy B. Arbogast. (2014) Evaluation of Pediatric ATD Biofidelity as Compared to Child Volunteers in Low-Speed Far-Side Oblique and Lateral Impacts. *Traffic Injury Prevention* 15 Suppl 1 (2014): S206-214.
- Snyder RG, Schneider LW, Owings CL, Reynolds HM, Golomb DH, Sckork MA. Anthropometry of Infants, Children, and Youths to Age 18 for Product Safety Design. Internet: [<https://deepblue.lib.umich.edu/handle/2027.42/684>], 1977.
- Wismans et al. (1979) Child Restraint Evaluation by Experimental and Mathematical Simulation, 23rd Stapp Car Crash Conf Proc, SAE #791017
- Yoganandan, N., Kumaresan, S., Pintar, F., & Gennarelli, T., 2002. Pediatric biomechanics. In: Nahum, A., & Melvin, J. (Eds.), *Accidental Injury*. Springer New York, pp. 550–587.
- Yoganandan, N., Pintar, F., Kumaresan, S., & Gennarelli, T. A. (2000). Pediatric and small female neck injury scale factors and tolerance based on human spine biomechanical characteristics. In *IRCOBI Conference* (pp. 345–359). Montpellier, France.